

# Mechanical properties of rat soleus aponeurosis and tendon during variable recruitment *in situ*

Ryan J. Monti<sup>1</sup>, Roland R. Roy<sup>2,\*</sup>, Hui Zhong<sup>2</sup> and V. R. Edgerton<sup>1,2</sup>

<sup>1</sup>Department of Physiological Science and <sup>2</sup>Brain Research Institute, University of California Los Angeles, Los Angeles, CA 90095-1761, USA

\*Author for correspondence (e-mail: rrr@ucla.edu)

Accepted 20 June 2003

## Summary

The *in vitro* mechanical properties of tendons are well described, whereas little data exist for conditions mimicking those found *in vivo*. Descriptions of the *in situ* mechanical properties of aponeuroses are more common, but the results are variable. Our goal was to examine the mechanical properties of these tissues under conditions mimicking the *in vivo* state. Tissue strains were measured in the rat (*Rattus norvegicus*) soleus muscle directly from the spacing of metal markers implanted within the tissues of interest using an X-ray video microscope. Strains were measured for the tendon and three regions (proximal, middle and distal) of the aponeurosis. Muscle stimulation was accomplished through isolated ventral rootlets, allowing force to be graded in seven repeatable increments independent of muscle–tendon unit length. Peak strains

(during maximal tetanic contraction at optimum length;  $P_0$ ) were ~5% in tendon and ~12% in all regions of the aponeurosis. At forces above 50% of  $P_0$ , tissue stiffness was nearly constant in all regions, and a pronounced toe region was observed only at forces below ~25% of  $P_0$ . Stiffness increased in all regions as the muscle–tendon unit was lengthened. These results suggest that using mechanical properties measured *ex vivo* or during single contractile events *in situ* to estimate the *in vivo* behavior of tendon and aponeurosis may lead to errors in estimating the distribution of strain among the contractile and series elastic elements of the muscle.

Key words: aponeurosis, tendon, muscle–tendon unit, tissue strain, tissue stiffness, soleus muscle, rat, *Rattus norvegicus*.

## Introduction

The *in vitro* mechanical properties of isolated mammalian tendons have been well characterized. Bennett et al. (1986) tested tendons associated with muscles having a variety of functions from seven species of animals including quadrupeds of different sizes, wallaby and dolphin. All tendons tested had similar Young's moduli (1.2–1.6 GPa), failed at similar stresses and had a similar capacity to store and return strain energy. This uniformity of tendon mechanical properties across species was confirmed in a comprehensive study by Pollock and Shadwick (1994), who demonstrated that the elastic modulus of tendons did not scale with body mass but remained relatively constant at near 1.2 GPa for 18 species of animals with body masses ranging from 0.5 kg to 500 kg. Furthermore, no differences were observed in the mechanical properties of tendons from flexors and extensors of the ankle joint, indicating that the mechanical properties of these tendons are not specialized with respect to the function of the attached muscle.

These Young's moduli, however, are tangent moduli measured from free tendons *in vitro*. Under conditions that either limit the applied load to maximal isometric tension ( $P_0$ ) or stimulate the muscle itself to load the tendon, a different picture emerges. The tendons of the cat soleus (Proske and Morgan, 1984; Scott and Loeb, 1995) and frog semitendinosus

(Lieber et al., 1991) remain within the early, non-linear region of their stress–strain curves when subjected to a range of forces up to  $P_0$ . Therefore, the use of a Young's modulus derived from the linear portion of an *in vitro* stress–strain curve may result in an underestimate of tendon extension during a movement, particularly at low levels of recruitment.

The relationship between strain and muscle–tendon unit (MTU) force or length is less clear. In general, two approaches have been used to study this relationship. Some studies have examined the properties of aponeurosis in response to passive loading (lengthening) of the specimens (Lieber et al., 1991; Trestik and Lieber, 1993; van Bavel et al., 1996). Generally, this involves stretching the MTU until the passive force is equal to a maximum tetanic contraction at optimum length ( $P_0$ ). Alternatively, some investigators have applied varying forces to the aponeurosis by modulating the contractile force of the muscle being studied (Ettema and Huijing, 1989; Maganaris and Paul, 2000a,b; Rack and Westbury, 1984; Zuurbier et al., 1994). Experiments using either of these methods represent a combination of variations in length and applied load and cannot separate the independent effects of force and MTU length on the mechanical properties of the connective tissues.

There is no clear consensus on the mechanical properties of the aponeurosis or on the relationship between tendon and aponeurosis mechanical properties in the literature. Rack and Westbury (1984) noted that the total stiffness of the connective tissue of the cat soleus was 3–5 times less during isometric contractions than that of the free tendon measured in isolation, indicating that the tendon was much stiffer than other connective tissue elements (i.e. the aponeurosis). Other reports in a variety of species have also indicated differences in the mechanical properties of the tendon and aponeurosis. Tendon strain is approximately three times the aponeurosis strain during maximum voluntary contraction in the human tibialis anterior muscle (Maganaris and Paul, 2000b) and is approximately four times higher at a passive load equal to  $P_0$  in the frog semitendinosus (Lieber et al., 1991). By contrast, some reports have indicated that the tendon and aponeurosis within a muscle have similar mechanical properties. Trestik and Lieber (1993) reported a 2% strain in both the tendon and aponeurosis of the frog gastrocnemius passively loaded to  $P_0$ . The aponeurosis and tendon of the cat soleus have also been reported to have similar stiffness during tetanic contractions (Scott and Loeb, 1995). It should be noted that the studies reporting similar or different mechanical properties for the tendon and aponeurosis include both passive and active loading, and thus the results cannot be attributed to differences in the methods used to load the tissue.

In some muscles, the stiffness of the aponeurosis is also non-uniform along its length. Strain in the portion of the aponeurosis furthest from the tendon has been reported to be five times greater than the portion closest to the tendon in the rat medial gastrocnemius during single loading events (Zuurbier et al., 1994). The percent strain at the muscular end of the aponeurosis is also three times greater than at the tendinous end in the frog semitendinosus (Trestik and Lieber, 1993) and human tibialis anterior (Maganaris and Paul, 2000b). Thus, not only do the properties of the tendon and aponeurosis vary relative to one another within individual muscles, but the mechanical properties of the aponeurosis may also vary along its length.

Given the wide range of techniques and animal models used in these studies, it is unclear what the independent effects of MTU length and muscle force production are on the properties of the tendon and aponeurosis. The overall purpose of the present study was to begin to resolve these issues. To achieve graded, repeatable contractions without altering the MTU length, we stimulated the muscle through isolated ventral root filaments. By stimulating these filaments independently or in combination, we achieved a series of 'recruitment' levels by altering the number of active muscle fibers. Thus, the same relative recruitment level could be achieved regardless of changes in muscle length, allowing independent measurement of the force and length dependence of the mechanical properties of the free tendon and aponeurosis. Tissue strains were tracked using X-ray videography of metal markers implanted directly into the tissue of interest. These markers were therefore integrated within the tissues, avoiding the

complicating effects encountered by other investigators when attaching markers to the surface of the aponeurosis and tendon (Scott and Loeb, 1995; van Bavel et al., 1996).

### Materials and methods

All experiments were performed on the soleus muscle of adult female Wistar rats (*Rattus norvegicus*;  $N=4$ ; body masses ranging from 238 g to 271 g). The soleus was chosen for the following reasons. The muscle has a relatively simple architecture, being unipennate with an angle of pennation of approximately  $5^\circ$  (Roy et al., 1985), which minimizes potential errors from the two-dimensional measurements of the movement of the markers implanted in the muscle (see below). The soleus is comprised predominantly of slow fibers (Ariano et al., 1973), which minimizes (1) any complicating effects that may be related to the isolation and stimulation of groups of fibers with differing fiber types and (2) the possibility of inducing muscle fatigue during the repeated tetanic contractions required to perform these experiments. All procedures used in this study were approved by the Animal Care and Use Committees of the University of California Los Angeles and the California Institute of Technology and followed the American Physiological Society Animal Care Guidelines.

#### *Intramuscular marker implantation*

All implant surgeries were performed under aseptic conditions at the University of California Los Angeles. A skin incision was made at the midline of the posterior surface of the right leg. The fascia covering the lateral gastrocnemius muscle was incised and the soleus muscle was exposed carefully, taking care not to disturb its innervation or blood supply.

To allow the strain of the connective tissue to be visualized, small ( $<100\ \mu\text{m}$ ) tungsten particles were implanted into the muscle immediately beneath the aponeurosis and into the tendon. The individual particles were placed into the tip of a 30-gauge hypodermic needle using fine forceps. A 1 ml disposable syringe was used as a holder for the needle. A slot about 2 cm long cut into the side of the syringe allowed a fine wire 'plunger' to be manipulated to push the particle out of the tip of the needle. The plunger consisted of a  $127\ \mu\text{m}$ -diameter stainless steel wire soldered to a second wire of  $300\ \mu\text{m}$  diameter. With the fine wire trimmed to the proper length, the change in wire diameter created a stop that prevented the tip of the wire from pushing further into the tissue than the bevel of the needle. A  $90^\circ$  bend in the larger wire allowed it to be manipulated through the slot in the syringe. When the needle was inserted into the tissue, the plunger was used to push the particle out of the barrel. The needle was then withdrawn, leaving the marker embedded in the tissue.

Approximately 15–20 particles were implanted in each muscle. The particles were arranged in a series of rows oriented in a medial–lateral plane and spaced at  $\sim 2$ – $3\ \text{mm}$ . A single particle was placed at the midline of the soleus tendon, as far

distally as it could be distinguished from the tendons of the gastrocnemii. One additional particle was placed in the tibia for use as a reference point during analysis of the video images. Fig. 1 is a captured video image showing the arrangement of the particles in one representative soleus muscle.

Following surgery, the rats were placed in an incubator maintained at 37°C and returned to their cages when fully recovered. Buprenorphine (0.03 mg kg<sup>-1</sup> body mass; i.p.) was given every 8–12 h for the first 48 h post-operatively. During the first three days following surgery, the rats were given ampicillin (100 mg kg<sup>-1</sup> body mass; per os). The animals were given at least 5 days to recover before the *in situ* testing (see below) to allow the insertion sites within the muscle to heal completely.

#### Preparation for *in situ* testing

All *in situ* testing and X-ray videography procedures were performed at the NASA Jet Propulsion Laboratory (Pasadena, CA, USA) under the administration of the California Institute of Technology. All animals were anesthetized with sodium pentobarbital (50 mg kg<sup>-1</sup>; i.p.). Reflex checks were performed regularly during the preparation and testing, and supplements (20% of the initial dose) were given as needed to maintain a deep level of anesthesia. The animal was warmed by a circulating water heating pad during all preparatory procedures.

The muscles of the tail, hip, thigh and leg were denervated with the exception of the soleus. A dorsal midline incision was made from approximately T10 to S2. The deep fascia was then opened and the spinal musculature removed, providing access to the vertebral column. A laminectomy was performed from T12 to L6 to allow full access to the spinal cord and spinal roots. The dura mater was left intact on the surface of the spinal cord at this stage. The area was then irrigated thoroughly with physiological saline, covered with saline-soaked cotton gauze, and the skin closed temporarily with clamps during the remaining preparatory surgery.

The tendon of the plantaris muscle was cut and the tendons of the gastrocnemii were separated from the soleus tendon as distally as possible and cut. All three muscles were moved proximally to provide access to the soleus muscle. A small piece of the calcaneus, with the soleus tendon attached, was cut free. A hole was made through the bone fragment to allow insertion of a 300 µm stainless steel wire that was used to attach the muscle to a lever system (Model 305B-LR; Aurora Instruments, Toronto, Ontario, Canada).

The animal was placed on an acrylic sheet heated by a circulating water pump, which was on risers attached to an acrylic base. The leg was clamped in place by a pair of screw-driven pins at both the proximal and distal ends of the tibia. With the leg clamped rigidly in place, a pool was formed from the skin of the leg and filled with heated mineral oil to maintain the muscle temperature and to prevent drying. A small piece of cotton soaked in oil was placed over the distal portion of the tendon as it exited the bath to keep it moist. The bath temperature was maintained at ~34°C by a radiant heat source.

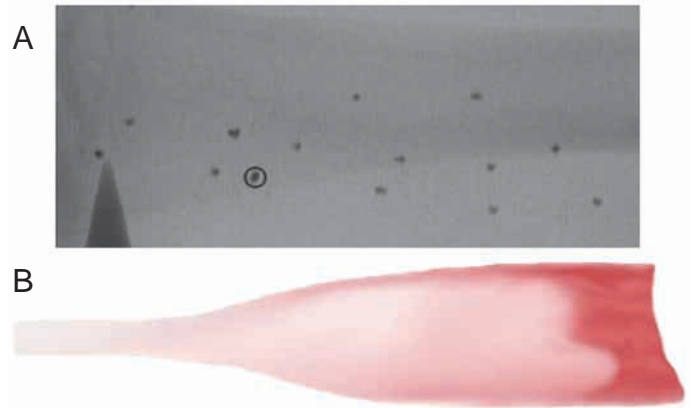


Fig. 1. (A) Captured video frame showing the typical spacing of the metal particles along the length of the tendon and aponeurosis. The circled particle is implanted in the tibia for use as a reference point to compensate for any limb movement. (B) Representation of the extent of the aponeurosis as a reference for the actual placement of the particles.

Clamps were then placed on the spinous process of one sacral vertebra and around the body of an upper thoracic vertebra to fix the spinal column.

Once the animal was secured on the testing platform, the dura was opened carefully along the length of the laminectomy. Using fine forceps, the dura was lifted to allow better visualization of the exit sites of the spinal roots. Ventral roots L4 to L6 were isolated and cut close to the spinal cord. Each root was stimulated to determine its contribution to soleus force-generating capability. With the roots contributing force to the soleus isolated, the skin of the back was used to form a pool for heated mineral oil. The innervation of the soleus muscle was derived from two roots in all animals, typically L5 and L6. The root contributing the greatest amount to the soleus (usually ~75%) was split, providing three ventral root bundles that could be stimulated separately or in combination to achieve seven different force levels. After confirming that the sum of the isolated roots agreed with whole muscle tension, direct stimulation of the tibial nerve rather than stimulation of all three ventral rootlets was used to elicit all whole-muscle contractions. Once a satisfactory preparation had been established, the apparatus holding the animal was transferred into the microscope.

#### *In situ* testing procedures

During the *in situ* testing procedures, the movement of the implanted particles was tracked using an X-ray microscope (FeinFocus USA, Inc., Simi Valley, CA, USA; Model FXS-160.30). This microscope provides an S-VHS output of the phosphor screen image, allowing the movement of the particles to be recorded on VHS tape at 60 fields s<sup>-1</sup>. All data were acquired using a laptop computer (Solo 9100; Gateway, Inc.) running custom software written in the LabView programming language (National Instruments, Austin, TX, USA). The computer controlled both the lever system and the

stimulator/stimulus isolator (Model S8800; Grass Instruments, Quincy, MA, USA) and recorded force and length data from the lever system. The video and digital data were synchronized using a digital timecode generator.

The optimum length for a whole muscle twitch contraction was determined and used as the start length for the testing procedure. All subsequent *in situ* testing was repeated for each of the seven possible combinations of ventral root bundles. Testing began with a series of whole-muscle isometric tetani performed in 1 mm increments to determine the optimum length for maximum tetanic tension ( $L_o$ ). This length was defined as  $L_o$  for all subsequent testing, regardless of the recruitment level being used. A length-tension relationship from 2 mm below  $L_o$  to 2 mm above  $L_o$  was determined for each of the seven recruitment levels. At the conclusion of the testing, a metal square of known dimensions was placed on the surface of the muscle and filmed as a distance calibration. The muscle length and temperature were measured and the animal was removed from the testing apparatus. The muscle was quickly frozen in isopentane cooled with liquid nitrogen and stored at  $-70^\circ\text{C}$  for histological analysis.

#### Data analysis

To assess the precise location of the implanted markers relative to the tissue of interest, cross-sections of frozen muscles were cut at 15  $\mu\text{m}$  intervals. Sections containing fragments of a marker were stained with hematoxylin and eosin and examined under a light microscope (Fig. 2). Typically,

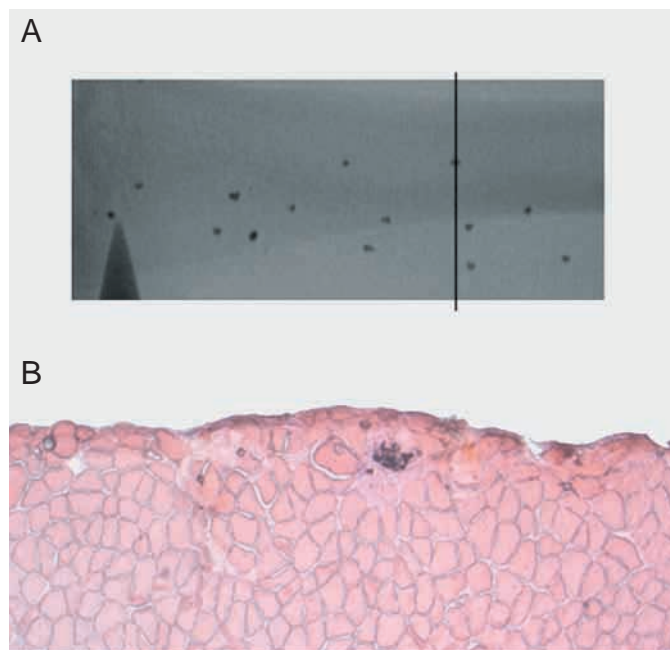


Fig. 2. (A) The same captured video frame shown in Fig. 1, indicating the level of the histological section shown in B. The section is stained with hematoxylin and eosin and illustrates the placement and encapsulation of the metal particle. Note that it is completely surrounded by connective tissue that is physically continuous with the aponeurosis.

particles were within 150  $\mu\text{m}$  of the surface of the muscle. In all cases, the particles were encapsulated by a thin layer of connective tissue, indicating that the area of the implant had healed during the recovery period. No signs of residual trauma from the implantation procedures were observed. The encapsulating connective tissue was continuous with the endomysium and aponeurosis. The presence of consistent encapsulation of the implants is important because it assured a stable position of the particles, thus making them accurate markers of the movement in the surrounding tissue.

All digital image analysis was performed with programs written using IMAQ Vision software (National Instruments). For each contraction, the corresponding sequence of video frames was acquired digitally and stored on disks. The boundaries of each implanted particle were determined programmatically. All pixels darker than the median for their row and column within a user-defined region surrounding the marker were defined as being part of the marker. The outline surrounding the pixels satisfying this criterion was defined as the boundary of the marker. From this boundary, the centroid of the marker was determined and used to compute all distances. Preliminary analyses indicated that this method yielded less frame-to-frame variability in the determination of particle position. However, some noise still exists in particle location due to signal degradation by the video capture system and fluctuations in phosphor intensity with time. These factors may cause subtle changes in the apparent outline of the particles, leading to small frame-to-frame differences in the calculation of the centroid. Measurement of video sequences showing particles at rest indicated that this noise is approximately one pixel width ( $\sim 20 \mu\text{m}$ ) at its peak (data not shown).

The longitudinal axis of the muscle was defined by measuring the mean path traced by each of the particles. This axis represents the path of shortening of the MTU as a whole. The movement of the markers was split into longitudinal and lateral components parallel or perpendicular to this axis. Longitudinal and lateral strains were computed based on the relative motion of any two particles along these respective axes. However, lateral strains were less than the pixel resolution of the video and are not reported. The initial spacing of the particles for strain computations was taken from the positions of the particles with the muscle at rest and 2 mm below  $L_o$ . Thus, zero strain was the same for any two contractions of an individual muscle. In general, the five rows of markers within the muscle allowed four segments to be identified by using the distance between alternate rows: proximal aponeurosis (PA), middle aponeurosis (MA), distal aponeurosis (DA) and proximal tendon/distal aponeurosis (PTDA). Additionally, the distance from the calcaneus to the marker in the proximal portion of the tendon provided strain measurements for the tendon (TEND).

#### Determination of tissue stiffness

Strain measurements based on the video images were made during the plateau of the tetanic contractions. Strain

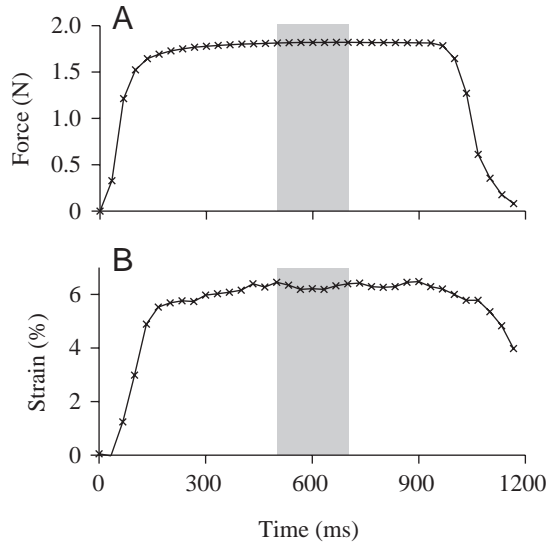


Fig. 3. Representative force (A) and strain (B) patterns for a single particle pair during a tetanic contraction. The mean force and strain from a series of video frames (shaded region; ~100 ms) were used to construct the force–strain curves for every particle pair studied.

measurements from three consecutive frames (100 ms) were averaged, as was the muscle force recorded over the same time period (Fig. 3). These values were used to create plots of tissue strain as a function of muscle force (Fig. 4). Strains were used rather than changes in the absolute distances between markers because marker spacing could not be kept constant among animals. One force–strain plot was created for each region of the muscle at each MTU length. The force–strain plots were best fit by an exponential curve of the form  $y=ae^{bx}$ . From the equation of the best fit line for each plot, the slopes of tangent lines could be computed at uniform force levels across all muscles, regardless of whether that precise force level was achievable by stimulation of the particular combination of ventral roots available in an animal (i.e. stiffness was computed at 25% or 75% of  $P_0$  for any animal for ease of comparison). These slopes represent the stiffness of the tissue at the chosen level of recruitment. Because strain was used rather than absolute displacements, and because stress cannot be computed between each particle pair, stiffness values in the study are reported as N/% strain using whole muscle force.

#### Statistical analysis

Effects of anatomical region and MTU length on strain and stiffness at  $P_0$  were assessed by two-way analysis of variance (ANOVA) with an alpha level of 0.05. When a significant group effect (region, length) was detected, data for regions or lengths were subjected to multiple paired comparisons using the Bonferroni adjustment at a group significance level of  $P<0.05$ . To test for effects of recruitment level, stiffness values within a single region at  $L_0$  were compared using a paired  $t$ -test (significance level  $P<0.05$ ).

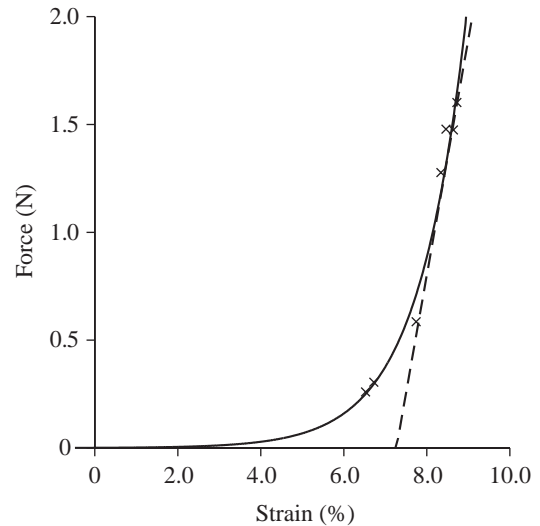


Fig. 4. A representative force–strain curve for a single pair of particles (middle aponeurosis;  $L_0$ ). Each point (x) is from a maximal tetanic contraction *via* a different combination of ventral root filament bundles. At the lowest recruitment levels used in this study (15–20% of  $P_0$ ), the strains were typically more than 50% of the strains attained at  $P_0$ . This implies the existence of a highly compliant toe region. The straight line is a tangent to the force–strain curve at 75% of  $P_0$ , and its slope is the stiffness of the tissue at that point.  $P_0$  for this muscle was 1.58 N. Thus, it can be seen from the relationship between this tangent line and the force–strain curve that the stiffness of the tissue did not vary much above ~30% of  $P_0$  (0.5 N for this muscle).

## Results

### Shape of the force–strain relationship

The relationship between muscle force and connective tissue strain exhibited a very compliant ‘toe’ region where strain increased rapidly at low forces followed by an abrupt stiffening, with the relationship approaching linear at high forces. This is shown for a single pair of particles in Fig. 4. Because of the nearly linear force–strain relationship at high recruitment levels, the curvilinear fit to the data required that the highly compliant, early portion of this relationship occurred at forces below those achieved in the preparations used in this study. The smallest ventral root bundles isolated recruited slightly less than 15% of the muscle, producing approximately 200 mN on average, approximately the force level at which the toe region becomes most pronounced.

### Length dependence of tissue properties

Peak strain (strain at  $P_0$ ) in all segments of the aponeurosis increased with lengthening of the MTU (Fig. 5), but this increase was significant only at 2 mm above  $L_0$  ( $P<0.05$ ). Tendon strain at  $P_0$  was similar at all MTU lengths and was approximately half that observed in the aponeurosis ( $P<0.05$ ). Total strain in all elements at  $P_0$  ranged from 9% to 12% and reached a plateau at lengths above  $L_0$  (Fig. 5). Stiffness

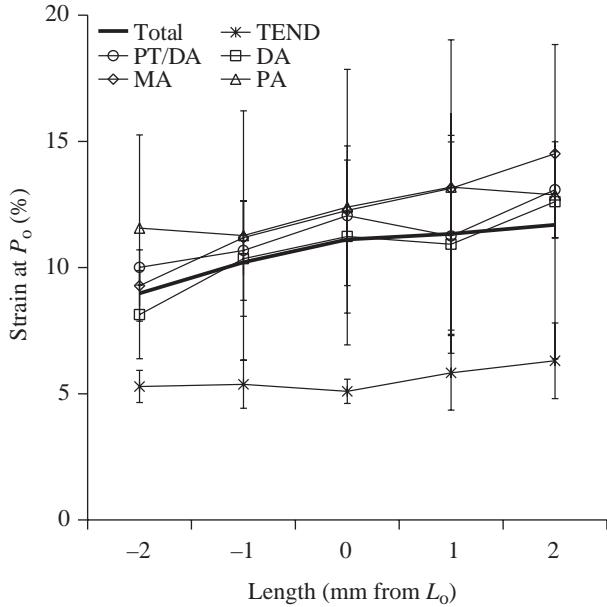


Fig. 5. The relationship between peak strain (strain at  $P_0$ ) and muscle-tendon unit (MTU) length for each of the five segments defined in this study: DA, dorsal aponeurosis; MA, middle aponeurosis; PA, proximal aponeurosis; PT/DA, proximal tendon/distal aponeurosis; TEND, tendon. Strains in the tendon were significantly ( $P < 0.05$ ) less than those in all regions of the aponeurosis and did not vary significantly with increasing MTU length. By contrast, peak strains in the aponeurosis tended to increase with lengthening of the MTU. Values are means  $\pm$  1 s.d. ( $N=4$ ).

generally increased with increasing MTU length in all tissue segments (Fig. 6) but, again, was significant only at 2 mm above  $L_0$  ( $P < 0.05$ ). The patterns for the various portions of the aponeurosis were very similar, with stiffness increasing slowly up to  $L_0$  and then more rapidly at lengths above  $L_0$ . For the tendon, stiffness appeared to plateau as MTU length increased. Paired  $t$ -tests with a Bonferroni adjustment for multiple comparisons indicate that the TEND is significantly stiffer than the DA, MA or PA ( $P < 0.05$ ) but not than the PTDA overlap region at all lengths.

*Force dependence of tissue properties*

Fig. 7 shows a comparison of the stiffness at  $L_0$  for each of the regions studied for two different levels of force production. As seen in Fig. 6, the tendon is stiffer than the aponeurosis and, after the first few mm (PTDA), the aponeurosis stiffness is uniform. Stiffness of the PTDA region is not significantly different from either the tendon or the remainder of the aponeurosis. Fig. 7 also illustrates the variation in tissue stiffness as a function of recruitment level. At a low recruitment level (25% of  $P_0$ ), the pattern of stiffness variation remains (TEND is still significantly stiffer), but each region is significantly more compliant at 25% of  $P_0$  than at  $P_0$  ( $P < 0.05$ ). The values for strain and stiffness at three recruitment levels are summarized in Table 1 for each region studied.

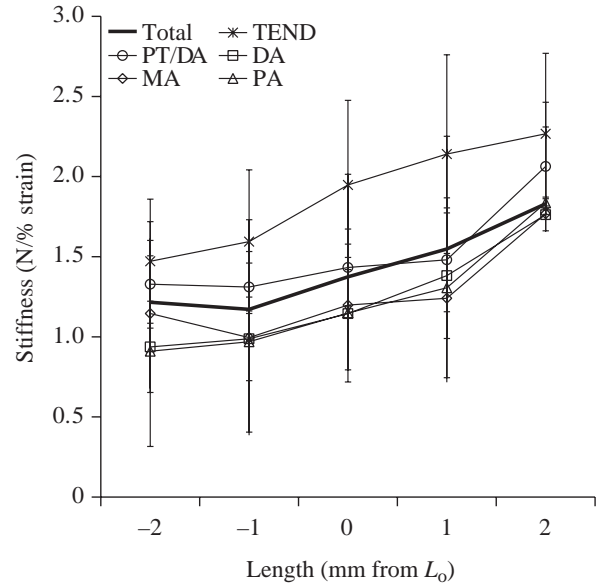


Fig. 6. The relationship between stiffness (N/% strain) and muscle-tendon unit (MTU) length for each of the five segments defined in this study; for definitions of abbreviations, see Fig. 5. Tendon stiffness was greater than that of all regions of the aponeurosis and did not vary significantly with increasing MTU length. The stiffness of the aponeurosis was relatively constant across lengths but was significantly ( $P < 0.05$ ) higher at  $L_0+2$  mm than at any other length. Values are means  $\pm$  1 s.d. ( $N=4$ ).

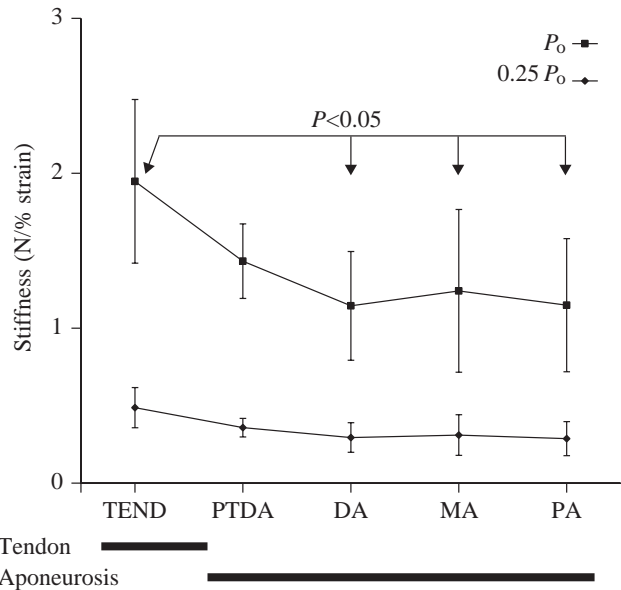


Fig. 7. Variations in stiffness among the five segments studied at  $P_0$  or 0.25 of  $P_0$ . Stiffness declines from the tendon to the aponeurosis, and the tendon was significantly ( $P < 0.05$ ; indicated on graph) stiffer than all three regions that did not include any overlap between tendon and aponeurosis. In addition, while the general pattern holds for contractions at 0.25 of  $P_0$ , the tissue is much more compliant. TEND, tendon; PTDA, proximal tendon/distal aponeurosis; DA, dorsal aponeurosis; MA, middle aponeurosis; PA, proximal aponeurosis.

Table 1. Strain and stiffness values for each region of the tendon and aponeurosis at  $L_o$ 

	Force	TEND	PTDA	DA	MA	PA
Strain (%)	$P_o$	5.10±0.48	12.05±2.77	11.23±3.03	12.27±1.94	12.39±5.46
	0.75 $P_o$	4.79±0.32	11.72±2.77	10.66±4.58	11.94±1.93	11.99±5.34
	0.25 $P_o$	3.64±0.28	10.44±2.78	9.38±4.50	10.67±1.93	10.47±4.89
Stiffness (N/% strain)	$P_o$	1.95±0.53	1.43±0.24	1.14±0.35	1.20±0.35	1.15±0.43
	0.75 $P_o$	1.46±0.97	1.07±0.18	0.87±0.31	0.90±0.40	0.86±0.47
	0.25 $P_o$	0.49±0.13	0.36±0.06	0.29±0.10	0.30±0.09	0.29±0.11

Values are means ± s.d.  
 DA, dorsal aponeurosis; MA, middle aponeurosis; PA, proximal aponeurosis; PT/DA, proximal tendon/distal aponeurosis; TEND, tendon;  $L_o$ , optimum length for maximum tetanic tension.

### Discussion

The present study examined the mechanical and contractile behavior of the rat soleus muscle under *in situ* conditions designed to mimic those encountered *in vivo*. Bundles of ventral root filaments were used to vary the recruitment level of the muscle through stimulation of subsets of muscle fibers rather than varying whole muscle stimulation parameters (frequency, voltage, etc.) or muscle length as used in previous studies (Ettema and Huijing, 1989; Huijing and Ettema, 1988; Scott and Loeb, 1995; Zuurbier et al., 1994). This method provides the advantage of (1) maintaining the same stimulus pattern during all measurements, (2) allowing force to be varied independent of length and (3) allowing the same groups of muscle fibers to be recruited repeatedly without adjusting for changes in neuron stimulation thresholds that alter the outcome of voltage-graded contractions. The stiffness of the tendon and aponeurosis was determined based on the movement of markers implanted directly into the tissues of interest in response to the forces applied by the muscles.

Tendon strains at peak muscle loads ( $P_o$  or maximum voluntary contraction) have been reported to be in the range of 2–5% (Lieber et al., 1991; Maganaris and Paul, 2000a,b; Muramatsu et al., 2001). In the present study, we observed strains in the rat soleus tendon of 5–6%, in agreement with these previous results. In addition, tendon strain was not sensitive to changes in MTU length near and above  $L_o$ . Peak aponeurosis strains reported in the literature have a wider range, from as low as ~1% (van Donkelaar et al., 1999) to as high as ~50% (Zuurbier et al., 1994), with most investigators reporting strains in the 3–10% range (Ettema and Huijing, 1989; Lieber et al., 1991; Maganaris and Paul, 2000a,b; Muramatsu et al., 2001; Zuurbier et al., 1994). The aponeurosis strains we observed were at the high end of this range, generally falling between 10% and 12%.

Because force was varied independent of muscle length by stimulating more or fewer ventral root bundles, the dependence of stiffness on the level of muscle recruitment was measured in the present study. The results (Fig. 7) showed that the aponeurosis and tendon are very compliant at low recruitment levels (0.3–0.5 N/% strain at 25% of  $P_o$ ) and that stiffness increases rapidly with enhanced recruitment. Above

~50% of  $P_o$ , the force–strain relationship became nearly linear (Fig. 4), with a constant tissue stiffness above this level of recruitment. In addition, it was only at forces near the lowest measured in this study (near or below 25% of  $P_o$ ) that stiffness declined significantly. Thus, the non-linear toe region frequently reported for low force levels was not apparent at forces greater than 25% of  $P_o$  in the rat soleus. These data contrast with reports for some muscles indicating that the tendon and aponeurosis act exclusively in the non-linear region of their force–strain relationship at loads typically encountered *in vivo* (Lieber et al., 1991; Scott and Loeb, 1995). However, there is some previous evidence for a transition in connective tissue behavior within the range of forces observed *in vivo*. By an extension of the  $\alpha$ -plot technique (Morgan, 1977), Proske and Morgan (1987) showed that at muscle forces below 20% of  $P_o$  the stiffness of the connective tissue in the cat soleus decreased rapidly. Direct measurement of cat soleus tendon and aponeurosis strain using surface-mounted sonomicrometry crystals showed a similar reduction in stiffness during contractions below 20% of  $P_o$  (Scott and Loeb, 1995). The shape of the toe region below 15% of  $P_o$  cannot be directly addressed in the present study because the lowest recruitment level achieved was at approximately that threshold value.

The possibility that the length of the MTU might have an influence on the connective tissue properties should be considered. The geometry of the collagen in the endomysium has been examined carefully. Described as a mesh of randomly oriented collagen fibrils when originally examined by electron microscopy (Borg and Caulfield, 1980; Rowe, 1981), more recent analysis has demonstrated that it is to some degree an ordered array of fibrils (Purslow and Trotter, 1994). At short MTU lengths, the arrangement of the collagen is biased toward circumferential, and as muscle length increases the fibrils become increasingly oriented with the long axis of the muscle (Purslow and Trotter, 1994; Tidball, 1986). The collagen network in the aponeurosis may behave similarly. Additionally, collagen fibrils at short lengths appear wavy, or crimped. As they are lengthened and straightened out, they will theoretically become stiffer. This behavior has been implicated as a possible reason for the observed non-linear increase in

strain with increasing force early during the extension of tendons *in vitro* (Diamant et al., 1972).

To our knowledge, this is the first study that has independently tested the effects of muscle force and MTU length on the mechanical properties of tendon and aponeurosis. When maximally stimulated at MTU lengths from 2 mm below to 2 mm above  $L_0$ , the strain observed in the aponeurosis, but not in the tendon, increased steadily (Fig. 5). Because a common particle spacing at rest was used for all strain measurements for each pair of markers, this trend cannot be due to an increase in the passive strain of the tissue and must be an inherent property of the tissue. In addition, the strain continued to increase at lengths above  $L_0$ , where the maximal force began to decline slightly as the muscle fibers moved onto the descending limb of their length–tension relationships. A similar result was obtained for the stiffness of all five regions studied, with stiffness values for all regions increasing by ~50% over the range of MTU lengths (Fig. 6). In rat extensor digitorum longus, a similar right-shift of the force–strain relationship with increased strains at a given level of force as the MTU was lengthened has been observed (Ettema and Huijing, 1989), but no variations in aponeurosis stiffness were observed. However, these authors used single tetanic contractions at multiple lengths to vary the force applied to the aponeurosis. Because most of their measurements were made below  $L_0$ , the increase in strain associated with an increase in length would be accompanied by an increase in muscle force, keeping the total ratio ( $F/\Delta L$ ) nearly constant.

One consideration in interpreting the results of the present study is that the reported relationships are force–strain and not stress–strain. The ambiguity in defining the cross-sectional area of the aponeurosis, combined with a contractile force generated by a variable population of muscle fibers, prevents the calculation of connective tissue stress. Therefore, the stiffness values reported are the apparent stiffness of the whole tissue or segment described, not a dimensionless stiffness as derived from *in vitro* testing. This apparent stiffness is an accurate representation of the *in vivo* behavior but may not reflect the absolute material properties of the tissues. When interpreting these results, it is necessary to consider the unique aspects of this preparation. First, because force was varied by maximally stimulating groups of muscle fibers, the stress exerted by the muscle belly was constant. This is true because each of the rootlets contained an approximately equal proportion of fast and slow motor units, so every increase in force was accompanied by a proportional increase in the total cross-sectional area of active fibers. This contrasts with protocols varying the activity of the whole muscle, where muscle stress would increase with muscle force. Second, the stress applied by the active muscle fibers may not be borne by the entire cross-section of the aponeurosis or tendon at submaximal recruitment levels, meaning that connective tissue stress may not be a simple function of muscle force. Because of this unique *in vivo*-like relationship between muscle stress and connective tissue stress, the observed force–strain relationship could be affected by the mechanics of the

interaction between motor units, or groups of motor units, and the connective tissues through which they exert their force (Monti et al., 2001). For the cat soleus muscle, a model assuming that all muscle fibers act on a common elasticity can account for most, but not all, of the non-linearity observed in the addition of forces from two populations of muscle fibers (Sandercock, 2000). Similarly, the relationship between the fraction of the muscle that is active and the fraction of the connective tissue that is loaded could affect the shape of the observed force–strain relationship.

Fig. 8 illustrates three hypothetical relationships between recruitment, the fraction of the connective tissue that is loaded by active muscle fibers and the resulting stress in the loaded connective tissues. As in the experiments performed in this study, the model only considers load imposed on the connective tissue by muscle fibers. External loads imposed on the muscle are ignored, and therefore parallel elastic elements are excluded from consideration. In Fig. 8A, the assumption is that with each additional muscle fiber recruited, an additional portion of the connective tissue is loaded. In essence, the connective tissue is ‘recruited’ along with (or in proportion to)

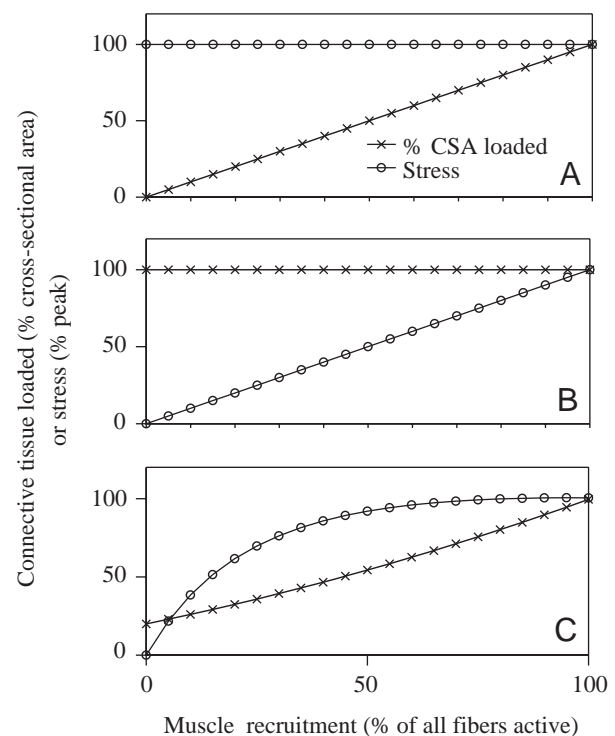


Fig. 8. Hypothetical relationships between muscle fiber and connective tissue recruitment. (A) All connective tissue is loaded at every recruitment level, leading to a linear increase in connective tissue stress with an increasing number of muscle fibers recruited. (B) The amount of connective tissue is a constant function of recruitment, leading to a constant stress in the connective tissue. (C) The amount of connective tissue recruited is disproportionately high at low forces, with an increase as force rises. This leads to a non-linear increase in connective tissue stress with recruitment. For details, see text.

the muscle fibers. Under this assumption, the connective tissue stress is constant. Thus, the transition from a highly compliant and variable behavior (the toe region) to a stiff and nearly constant behavior would require a transition between the properties of the connective tissues loaded at low and high recruitment levels. Fig. 8B illustrates the inverse of this relationship, a situation similar to that proposed by Sandercock (2000). Here, every muscle fiber is functionally in series with all of the connective tissues, and the connective tissue stress therefore rises as a linear function of muscle fiber recruitment. Under this assumption, the intrinsic stress-strain properties of the connective tissues would be the same as the observed force-strain relationship. The third model (Fig. 8C) is a combination of the first two. The assumptions are that initially there is some portion of the connective tissue that is loaded by any active muscle fibers (model 1) but that additional connective tissue is loaded as more fibers are recruited (model 2). In this third model, the sharp transition in the force-strain properties observed in this study, with a nearly constant stiffness at higher recruitment levels, can result from a much shallower stress-strain relationship with a constantly varying stiffness. Thus, the properties of the connective tissues as loaded *in vivo* may be more uniform than would be predicted from the stress-strain relationships.

The results of this study suggest that the mechanical properties of tendon and aponeurosis measured *ex vivo*, or *in situ* during isolated contractile events, may not represent the properties of these tissues during normal loading *in vivo*. Instead, we have observed a nearly constant stiffness as load increased due to muscle recruitment. The difference between our data and published descriptions of the *in vitro* properties of tendon may be accounted for by some very simple assumptions about the interface between the contractile elements of the muscle and the connective tissues. If the true stiffness of the tissues increases with recruitment, then the apparent, and functional, stiffness remains constant. By providing a series elasticity of nearly constant stiffness, the control of the muscle would be greatly simplified because the nervous system would not have to adjust to a constantly changing interface with the environment.

The authors thank Mr James Weiss, Mr Frank Hartley and Mr David Mih at the NASA Jet Propulsion Laboratory for providing access to the X-ray video microscope. This study was supported by National Institutes of Health Grant NS16333.

### References

- Ariano, M. A., Armstrong, R. B. and Edgerton, V. R. (1973). Hindlimb muscle fiber populations of five mammals. *J. Histochem. Cytochem.* **21**, 51-55.
- Bennett, M. B., Ker, R. F., Dimery, N. J. and Alexander, R. McN. (1986). Mechanical properties of various mammalian tendons. *J. Zool. Lond. A* **209**, 537-548.
- Borg, T. K. and Caulfield, J. B. (1980). Morphology of connective tissue in skeletal muscle. *Tissue Cell* **12**, 197-207.
- Diamant, J., Keller, A., Baer, E., Litt, M. and Arridge, R. G. (1972). Collagen; ultrastructure and its relation to mechanical properties as a function of ageing. *Proc. R. Soc. Lond. B. Biol. Sci.* **180**, 293-315.
- Ettema, G. J. and Huijing, P. A. (1989). Properties of the tendinous structures and series elastic component of EDL muscle-tendon complex of the rat. *J. Biomech.* **22**, 1209-1215.
- Huijing, P. A. and Ettema, G. J. (1988). Length-force characteristics of aponeurosis in passive muscle and during isometric and slow dynamic contractions of rat gastrocnemius muscle. *Acta Morphol. Neerl. Scand.* **26**, 51-62.
- Lieber, R. L., Leonard, M. E., Brown, C. G. and Trestik, C. L. (1991). Frog semitendinosus tendon load-strain and stress-strain properties during passive loading. *Am. J. Physiol. Cell Physiol.* **261**, C86-C92.
- Maganaris, C. N. and Paul, J. P. (2000a). *In vivo* human tendinous tissue stretch upon maximum muscle force generation. *J. Biomech.* **33**, 1453-1459.
- Maganaris, C. N. and Paul, J. P. (2000b). Load-elongation characteristics of *in vivo* human tendon and aponeurosis. *J. Exp. Biol.* **203**, 751-756.
- Monti, R. J., Roy, R. R. and Edgerton, V. R. (2001). Role of motor unit structure in defining function. *Muscle Nerve* **24**, 848-866.
- Morgan, D. L. (1977). Separation of active and passive components of short-range stiffness of muscle. *Am. J. Physiol. Cell Physiol.* **232**, C45-C49.
- Muramatsu, T., Muraoka, T., Takeshita, D., Kawakami, Y., Hirano, Y. and Fukunaga, T. (2001). Mechanical properties of tendon and aponeurosis of human gastrocnemius muscle *in vivo*. *J. Appl. Physiol.* **90**, 1671-1678.
- Pollock, C. M. and Shadwick, R. E. (1994). Relationship between body mass and biomechanical properties of limb tendons in adult mammals. *Am. J. Physiol. Reg. Integ. Comp. Physiol.* **266**, R1016-R1021.
- Proske, U. and Morgan, D. L. (1984). Stiffness of cat soleus muscle and tendon during activation of part of muscle. *J. Neurophysiol.* **52**, 459-468.
- Proske, U. and Morgan, D. L. (1987). Tendon stiffness: methods of measurement and significance for the control of movement. A review. *J. Biomech.* **20**, 75-82.
- Purslow, P. P. and Trotter, J. A. (1994). The morphology and mechanical properties of endomysium in series-fibred muscles: variations with muscle length. *J. Muscle Res. Cell Motil.* **15**, 299-308.
- Rack, P. M. and Westbury, D. R. (1984). Elastic properties of the cat soleus tendon and their functional importance. *J. Physiol. Lond.* **347**, 479-495.
- Rowe, R. W. (1981). Morphology of perimysial and endomysial connective tissue in skeletal muscle. *Tissue Cell* **13**, 681-690.
- Roy, R. R., Baldwin, K. M., Martin, T. P., Chimarusti, S. P. and Edgerton, V. R. (1985). Biochemical and physiological changes in overloaded rat fast- and slow-twitch ankle extensors. *J. Appl. Physiol.* **59**, 639-646.
- Sandercock, T. G. (2000). Nonlinear summation of force in cat soleus muscle results primarily from stretch of the common-elastic elements. *J. Appl. Physiol.* **89**, 2206-2214.
- Scott, S. H. and Loeb, G. E. (1995). Mechanical properties of aponeurosis and tendon of the cat soleus muscle during whole-muscle isometric contractions. *J. Morphol.* **224**, 73-86.
- Tidball, J. G. (1986). Energy stored and dissipated in skeletal muscle basement membranes during sinusoidal oscillations. *Biophys. J.* **50**, 1127-1138.
- Trestik, C. L. and Lieber, R. L. (1993). Relationship between Achilles tendon mechanical properties and gastrocnemius muscle function. *J. Biomech. Eng.* **115**, 225-230.
- van Bavel, H., Drost, M. R., Wielders, J. D., Huyghe, J. M., Huson, A. and Janssen, J. D. (1996). Strain distribution on rat medial gastrocnemius (MG) during passive stretch. *J. Biomech.* **29**, 1069-1074.
- van Donkelaar, C. C., Willems, P. J. B., Muijtjens, A. M. M. and Drost, M. R. (1999). Skeletal muscle transverse strain during isometric contraction at different lengths. *J. Biomech.* **32**, 755-762.
- Zuurbier, C. J., Everard, A. J., van der Wees, P. and Huijing, P. A. (1994). Length-force characteristics of the aponeurosis in the passive and active muscle condition and in the isolated condition. *J. Biomech.* **27**, 445-453.